REPORT DOCUMENTATION PAGE

Form Approved
OMB No. 0704-0188

1. REPORT DATE *(DD-MM-YYYY)*	2. REPORT TYPE	3. DATES COVERED *(From - To)*
December 10, 2008	Interim	June 14, 2008 – December 10, 2008

4. TITLE AND SUBTITLE
Effects of Subzero Temperatures and Seawater Immersion on Damage Initiation and Growth in Sandwich Composites.

5a. CONTRACT NUMBER
N/A

5b. GRANT NUMBER
N00014-07-1-0418

5c. PROGRAM ELEMENT NUMBER
N/A

6. AUTHOR(S)
Davidson, Barry, D.

5d. PROJECT NUMBER
N/A

5e. TASK NUMBER
N/A

5f. WORK UNIT NUMBER
N/A

7. PERFORMING ORGANIZATION NAME(S) AND ADDRESS(ES)
Syracuse University
Department of Mechanical and Aerospace Engineering
149 Link Hall
Syracuse, New York 13244

8. PERFORMING ORGANIZATION REPORT NUMBER
N/A

9. SPONSORING/MONITORING AGENCY NAME(S) AND ADDRESS(ES)
Yapa D. S. Rajapakse
Office of Naval Research
875 North Randolph Street
Arlington, VA 22203-1995

10. SPONSOR/MONITOR'S ACRONYM(S)
N/A

11. SPONSOR/MONITOR'S REPORT NUMBER(S)
N/A

12. DISTRIBUTION/AVAILABILITY STATEMENT
Approved for public release; distribution unlimited.

13. SUPPLEMENTARY NOTES
N/A

14. ABSTRACT
Progress during the past six months is described on the project "Effects of Subzero Temperatures and Seawater Immersion on Damage Initiation and Growth in Sandwich Composites." Efforts during this period have focused on (1) assessing the effects of environment and impact damage on the flexural response of sandwich laminates, (2) finalizing the improved modified peel test and associated data reduction method for determining the debonding toughness of sandwich structures, and (3) using this new test to assessment the toughness of sandwich structures with different face sheet materials under a variety of environments. In the first focus area, the proposed test matrix has been completed and the data obtained are used to draw a number of conclusions about the effects of temperature, sea water saturation, and impact damage on the static strength, static stiffness, fatigue strength, fatigue stiffness and life of sandwich laminates. Work in the second and third focus areas has been complcted. This work has been documented in one publication and a second is in preparation.

15. SUBJECT TERMS
Sandwich, composites, freezing, temperature, seawater, fracture, impact, fatigue, dynamic

16. SECURITY CLASSIFICATION OF:			17. LIMITATION OF ABSTRACT	18. NUMBER OF PAGES	19a. NAME OF RESPONSIBLE PERSON
a. REPORT	b. ABSTRACT	c. THIS PAGE			Barry D. Davidson
U	U	U	UU	34	19b. TELEPHONE NUMBER *(Include area code)* 315-443-4201

Effects of Subzero Temperatures and Sea water Immersion on Damage Initiation and Growth in Sandwich Composites
Interim Report for the period June 14, 2008 – December 10, 2008

Barry D. Davidson
December 10, 2008

Executive Summary

Progress during the past six months is described on the project "Effects of Subzero Temperatures and Sea water Immersion on Damage Initiation and Growth in Sandwich Composites." Efforts during this period have focused on (1) assessing the effects of environment and impact damage on the flexural response of sandwich laminates, (2) finalizing the improved modified peel test and associated data reduction method for determining the debonding toughness of sandwich structures, and (3) using this new test to assessment the toughness of sandwich structures with different face sheet materials under a variety of environments. In the first focus area, the proposed test matrix has been completed and a few final follow-up tests are currently being performed to address areas where there is large scatter in the data or where unexpected behaviors were observed. The data obtained are used to draw a number of preliminary conclusions about the effects of temperature, sea water saturation, and impact damage on the static strength, static stiffness, fatigue strength, fatigue stiffness and life of sandwich laminates. Work in the second and third focus areas has been completed. One publication has been prepared documenting the results of focus area (2) and will appear in "Major Accomplishments in Composite Materials and Sandwich Structures – An Anthology of ONR Sponsored Research," edited by I.M. Daniel, E.E. Gdoutos, and Y.D.S. Rajapakse. Work is currently underway documenting the results of focus area (3) in the form of a paper for archival journal publication.

Introduction

As described above, research efforts have focused on (1) the effects of environment and impact on the bending response of sandwich laminates, (2) debonding test development, and (3) toughness assessments. Details on these efforts, their current status, and the plans for completion are provided in the ensuing sections.

Bending Test Program

Test Geometries

As described in previous interim reports, the sandwich panels used in this investigation utilized 12.7mm thick Diab H100 core with 8 ply glass/vinylester face sheets with a $[0/90/0/90]_s$ stacking sequence. All sandwich panels were manufactured via vacuum assisted resin transfer using BGF 7532 plain weave glass fabric and Dow Chemical's Derakane 411-350 vinyl ester resin. Each panel that was manufactured was cut into eight 25.4mm wide specimens. These specimens were tested in four-point bending with a combined metal and rubber load pad spanning the inner loading heads. The test geometry is illustrated schematically in Figure 1. Specimens were tested in undamaged and impact damaged configurations. The impact damage level was chosen as 10J, and was induced via a 25mm diameter, cylindrically shaped impact head dropped through a guide tube to impact the specimen at the desired location. This was accomplished via a 2.67kg impactor and a drop height of 382mm. The impactor was captured upon its first rebound, such that only a single impact occurs on any given drop.

The impact fixture is shown schematically in Figure 2. Specimens were fully supported along their base during impact. Impacts were always introduced so that they were in the middle of the half-span, i.e., mid-way between the loading and support head on one side during testing. Further, the impact-damaged location was always on the upper, compressive side of the specimen during the test. Additional details on the test geometry, the loading and impact fixtures, and on specimen manufacturing are presented in our previous interim report.

Test Environments and Test Matrix

A total of four test environments were considered: 20°C dry, 20°C wet –20°C dry and –20°C wet. Here and subsequently, the term "wet" is used to denote a sea water saturated specimen. Sea water saturation was performed prior to testing and was done with a minimum of three months immersion of the specimen at room temperature. The details of this process are presented in the interim report for the previous period of work. All testing was done in air at the desired temperature.

Under each environment, both undamaged and impact damaged tests were conducted. This leads to the following eight test conditions and their associated abbreviations:

LTDU – low temperature (-20°C) dry undamaged
LTDD – low temperature (-20°C) dry damaged

LTWU – low temperature (-20°C) wet (sea water saturated) undamaged
LTWD – low temperature (-20°C) wet (sea water saturated) damaged

RTDU – room temperature (20°C) dry undamaged
RTDD – room temperature (20°C) dry damaged

RTWU – room temperature (20°C) wet (sea water saturated) undamaged
RTWD – room temperature (20°C) wet (sea water saturated) damaged

A minimum of two static and three fatigue tests were initially conducted at each condition. This yields an initial matrix of 8 conditions x 5 specimens/condition = 40 specimens, plus a significant number of additional specimens for exploratory testing (described in the previous interim report). In order to maintain a consistent influence of the effects of panel-to-panel variations, at any condition, the specimens used for the first two static tests were taken from different panels (here, "panel" is used to denote the 305mm long x 230mm wide plate that was manufactured and subsequently cut into 8 specimens). Similarly, the specimens used for the first three fatigue tests at any condition were also taken from different panels. In addition, in order to maintain reasonably uniform specimen quality, only specimens from sandwich panels that yielded 8 "high quality" specimens were used. That is, if a panel had ***any*** dry spots or other manufacturing defects, specimens from that panel were either scrapped or used only for exploratory specimens. As a result, a total of 18 panels were manufactured, out of which 9 "good" panels were obtained. Considering these 9 good panels (72 specimens) only, the specimen thickness varied from a minimum of 16.3mm to a maximum of 17.5mm with an average of 17.0mm and a standard deviation of 0.31mm.

Due to the long time period required for saturation, approximately 50% of the specimens were immersed in sea water shortly after they were manufactured. In some cases, one-half of the specimens from a given plate were chosen for immersion, whereas in other cases all specimens from a given plate were chosen. These selections were based upon timing considerations (i.e., since dry specimens were immediately ready to test, one of the early panels was devoted to this and all specimens from a later panel were immersed) as well as the "balancing" of the entire test matrix to eliminate panel-to-panel variations as described above (i.e., only one test per condition from any one panel). For those panels from which only half the specimens were sea water saturated, those selected constituted every-other-one from the cutting process, i.e., the specimens chosen were spread across the entire width of the original panel, rather than being chosen from just one side. In this way, any effects of spatially-varying properties within a given panel were minimized.

In addition to the initial test matrix of 40 experiments, a limited number of additional static and fatigue tests were (and continue to be) performed for those conditions where there was large scatter in the data or where unexpected behaviors were observed. This is described subsequently,

Static Tests

All static tests were run in displacement control at a loading rate of 0.025mm/s until failure. Figure 3 presents typical load versus displacement plots, and Figure 4 shows the primary test results: failure strength and failure mode. That is, this figure presents the core shear stress and face sheet stress at failure as well as information on the failure modes that were observed. All stresses were determined based on the measured total thickness and computed face sheet thickness for that individual specimen. In this and subsequent figures, the discrete symbols represent the average result from a given condition, and the error bars reflect the minimum and maximum values obtained. All of the static test data that is presented is based on two specimens per condition. The solid lines in the figure are included solely as an aid in visualizing the data.

Figure 4 shows that both the static failure strength and the static failure *mode* may be influenced by environment. For both wet and dry specimens, strength is observed to increase with decreasing temperature in both the undamaged and impact damaged conditions. At low temperature, there is no effect of sea water saturation, impact damage, or their combined effects on strength. However, there was potentially a failure mode transition for the LTWU specimens, with one specimen failing by core shear and one by face sheet compression. In fact, 3 other specimens, taken from plates that exhibited dry spots, all failed by face sheet compression when tested statically in the LTWU condition. For this reason, 1-2 additional static tests will be performed at this condition.

At room temperature, there is no effect of impact damage on strength in either the wet or dry condition. There is perhaps a slight effect of moisture on strength, with the dry specimens of a given damage mode perhaps being a bit stronger than the corresponding specimens that were moisture saturated. In addition, a failure mode transition was seen from dry to wet, with both

RTWD and one RTWU specimen failing by face sheet compression, and one RTWU specimen failing by core shear. Three other specimens, taken from plates that exhibited dry spots, were tested in the RTWU condition and resulted in two face sheet compression and one core shear failure. An additional test using a "good specimen" is planned at this condition.

Figure 5 presents the ratio of the stress at the nonlinear point to the ultimate strength as a function of condition, where the nonlinear point was obtained by visual means. This ratio is very consistent across specimens. The slightly larger values for the RTDD, RTWU and RTWD specimens are likely primarily a result of their lower ultimate strengths. Other than that, there is no apparent trend created by the influences of temperature, moisture or damage. We point out that no error bars are evident at the LTWU condition because the two specimens tested had the same ratio of nonlinear to ultimate stress.

Figure 6 shows normalized stiffnesses from the static tests as a function of condition. Here, stiffness is defined as the slope of the load versus deflection plot, as obtained within the linear region, divided by the specimen's width (i.e., stiffness = [load/width]/deflection). All results in the figure are normalized by the average stiffness from the LTDU specimens, which was found to be 5.59 MPa. With the exception of the dry undamaged specimens, decreasing the temperature is observed to produce an increase in stiffness. Comparing LTDU to LTWU and RTDU to RTDW, it appears that the wet undamaged specimens are less stiff than the dry undamaged specimens. However, a similar comparison for the damaged specimens indicates that there is no effect of moisture on the damaged stiffness. The low temperature wet specimens show a higher stiffness in the damaged than the undamaged condition, the room temperature dry specimens show a decrease in stiffness due to damage, and no effect of impact damage is observed for the other two specimen types.

Fatigue Tests

As described in previous interim reports, fatigue tests were performed at a frequency of 4 Hz and with a minimum fatigue load that is 10% of the maximum value (i.e., R=0.1). For all of the low temperature specimens, the maximum load per unit width was 45,700 N/m, which corresponds to a maximum core shear stress of approximately 1.54 MPa and a maximum face sheet stress of approximately 113 MPa (i.e., depending on the precise specimen dimensions). Considering the strength data of Figure 4, this corresponds to 68-70% of the static strength of specimens in all four conditions. All room temperature tests were performed at a maximum load level of 36,000 N/m. This corresponds to 65-70% of the static strength at each condition, and corresponds to 79% of the peak stress level at which the low temperature tests were conducted.

All fatigue tests were run in load control. Initial values of dynamic stiffness were measured using a similar approach as for the static tests. Here, dynamic stiffness is defined as $(\Delta P/B)/\Delta\delta$, where ΔP is the difference between the maximum and minimum load, B is the specimen's width, and $\Delta\delta$ is the measured displacement that occurs over the cyclically applied ΔP. The initial dynamic stiffness was measured at approximately 500 cycles in order to allow the test to stabilize. Displacement triggers were used to provide periodic stops as well as to indicate specimen failure. For stops at which failure did not occur, dynamic stiffness was recorded approximately 500 cycles after the test is restarted. This allowed the stiffness change to be recorded as a function of the number of loading cycles.

Figure 7 presents the normalized maximum core shear stress versus number of cycles to failure as a function of condition. Here, the core shear stress was computed for each specimen based on its exact fatigue load and dimensions. The normalization constant is 2.21 MPa, which corresponds to the average static ultimate core shear stress from the LTDU and LTDD specimens. Three specimens were tested at each condition except for LTWU, where four specimens were tested. All specimens failed by core shear.

Figure 7 shows that, within the experimental scatter, there is little difference in fatigue life between the LTDU and the LTWU specimens. There is also little difference in life for the LTDD and the LTWD specimens. Thus, it appears that moisture has no effect on life at -20C. However, the LTDU and LTWU both have significantly longer lives than the LTDD and LTWD specimens. Thus, although impact damage had essentially no effect on static strength (Figure 4), Figure 7 shows that it causes a significant reduction in fatigue life. The mean fatigue life of the LTDU and LTWU specimens is 214,724 cycles. The mean life for the LTDD and LTWD specimens is only 36% of this, at 77,602 cycles. Thus, low temperature impact damaged specimens have a fatigue life that is only about one-third that of low temperature undamaged specimens.

Considering the room temperature results, Figure 7 indicates that moisture has a deleterious effect on the life of the impact damaged specimens, but does not affect the undamaged specimens. That is, the mean life of the RTDD specimens is approximately 1.7 times that of the RTWD specimens, whereas the mean lives of the RTDU and RTWU specimens are essentially the same. Similar to the low temperature specimens, impact damage causes a significant reduction in fatigue life for both dry and wet specimens. The damaged room temperature wet specimens have a mean fatigue life that is only 36% of the RTWU life, and the RTDD specimens have a life that is 62% of the RTDU life. Thus, impact damage has the least effect in the room temperature dry condition, where it causes a 38% reduction in life. At the room temperate wet, low temperature wet and low temperature dry conditions, it causes a 64% reduction in life.

We point out that, if the data of Figure 7 were normalized with respect to ultimate strength at the same condition as the fatigue test is run, then all of the data points would fall on essentially the same horizontal line. Thus, when considering the life of specimens fatigue loaded at the same percentage of their ultimate strength, the room temperature specimens will show a longer life at any condition. However, this normalization is somewhat misleading, and for this reason the normalization with respect to a constant stress value was selected. For example, additional data, not presented in Figure 7, comes from two exploratory tests conducted at "-40°C." That is, these tests were begun at -40°C, but by the end the temperature had increased to the range of -21 to -25°C (due to specimen heat-up and the resulting heat input into the environmental chamber). The load for these tests was similar to that used for the RTDU and RTDD tests. One of these tests was stopped after 2.1M cycles with no failure, and the other specimen failed at 950,000 cycles. The data are not included in the plot due to the temperature fluctuation during the test. However, these results, and those in Figure 7, strongly support the assumption that fatigue life at a constant stress level increases with decreasing temperature.

Figure 8 presents typical plots of dynamic stiffness versus number of loading cycles for each type of specimen tested to-date, and Figure 9 presents the ratio of the final to the initial dynamic stiffness. In Figure 9, the symbols represent the mean of the specimens tested at each condition, and the error bars present the minimum and maximum values. From Figures 8 and 9, it may be observed that there is very little change in stiffness in the low temperature specimens in comparison to those at room temperature. In general, the stiffness change in the room temperature specimens occurred very close to failure.

Conclusions and Next Steps

The conclusions from the sandwich panel bending tests performed to-date are as follows:

- Environmental conditions that range from -20°C to room temperature and from dry to sea water saturated may affect the bending strength, stiffness and/or failure mode of composite sandwich structure. This has important implications for the accurate determination of material properties and points out the need for highly accurate failure models that are applicable across a range of usage environments.
- Dry sandwich structure tends to get stiffer and stronger as the temperature decreases from room temperature to -20°C.
- Impact with a 25.4mm diameter indentor at an energy level of 10J produced essentially no change in static strength. However, it resulted in a significant decrease in fatigue life: under room temperate wet, low temperature wet and low temperature dry conditions, this impact caused a 64% reduction in life. In the room temperature dry condition, it resulted in a 38% reduction in life. Thus, the results of static tests cannot be used to infer fatigue behaviors.
- Fatigue life at a given stress level appears to increase with decreasing temperature.

The remaining work in this area consists of:

- One additional static test under LTWU and RTWU to further examine the failure mode transition that is observed in these conditions.
- A few additional fatigue tests using the remaining specimens to examine either (1) specimen-to-specimen variability for specimens taken from the same panel and tested under the same conditions and/or (2) comparison between room temperature and low temperature results when tested at the same stress level.

Sandwich Debonding Test Assessment and Development

This work has been completed and has resulted in the development of an improved test and data reduction method for the modified peel test, shown schematically in Figure 10. These results have been documented in a paper entitled "An Improved Methodology for Measuring the Interfacial Toughness of Sandwich Beams" that will appear in *Major Accomplishments in Composite Materials and Sandwich Structures – An Anthology of ONR Sponsored Research*, edited by I.M. Daniel, E.E. Gdoutos, and Y.D.S. Rajapakse. The complete paper is presented in the Appendix of this report.

Effects of Environment on Debonding Toughness

Overview

In this task, experiments were performed on sandwich panel specimens to assess the effects of low temperature and sea water immersion on the debonding toughness of sandwich structure. All specimens used 25.4mm thick DIAB H100 core, 12 ply thick face sheets in a $[0/90/0/0/90/0]_s$ sequence, where 0° is defined to be the warp direction, and Dow Chemical's Derakane 411-350 vinyl ester resin. Glass reinforced laminates were fabricated using BGF 7532 plain weave glass fabric with an areal weight of 241 g/m^2, and carbon reinforced laminates were fabricated using Cytec-Fiberite W-5-322 T300 carbon fabric with an areal weight of 195 g/m^2. All laminates were fabricated as 230mm square panels using a vacuum assisted resin transfer molding process and contained a 12.7μm thick teflon insert between one face sheet and the core to serve as a starter crack. Following manufacture, panels were cut into 25mm wide test specimens using a band saw. Similar to the philosophy adopted for the bending tests, specimens were only taken from those panels that exhibited high manufacturing quality. Specimens taken from panels that exhibited dry spots were used only for exploratory testing.

Glass specimens were tested at -40C, -20C, 0C and 20C in both wet (sea water saturated) and dry conditions. Wet and dry carbon specimens were tested at 20C (room temperature) only. All sea water saturation was performed following the same technique adopted for the bending specimens. All tests were performed using the modified peel (MP) test and the debonding toughness, G_c, was found by the modified beam theory – load-displacement method of data reduction (described in the Appendix). Mechanically attached loading hinges were employed following the methodology described in the Appendix. All specimens had initial crack lengths of approximately 25mm. However, as described in the Appendix, the exact point of onset of advance from the teflon insert could not be identified, so this value was not used for the determination of toughness. Rather, when presenting resistance (G_c vs Δa) curves, the first crack length corresponds to the first time the test was stopped.

For the glass specimens, three specimens were tested in the -40C dry condition and four specimens were tested in all others. All of these specimens came from two different panels. For the -40C dry condition, one specimen was tested from panel 1 and two specimens were tested from panel 4. For all other conditions, two specimens were tested from each panel.

For the graphite specimens, four specimens were tested in the dry condition, which were comprised of two specimens from panel 2 and two from panel 3. Five tests were attempted in the wet condition. However, in two of these specimens, the cracked portion failed by compression early in the test, and in one, the initial crack jump was too long to obtain sufficient data for the data reduction method. Thus, the results from two "good" tests are available – one specimen from each panel.

Figure 11 presents the results from the room temperature tests. Note that the resistance (R) curves from all conditions are relatively flat. It can be observed that there is relatively little difference in the dry versus the wet toughness of the glass sandwich laminates, that the glass laminates are significantly tougher than the graphite laminates, and that the sea water saturated graphite laminates are tougher than the dry graphite laminates. The nature of crack advance is depicted in Figure 12. For the specimens with glass face sheets, growth occurred within the core paralleling the interface. However, interfacial growth, with some delamination at large crack lengths, occurred in the graphite reinforced specimens. The different type of growth accounts for the different toughnesses evidenced in Figure 11. We point out that the fiber sizing on the graphite specimens was vinylester compatible, but was not specifically designed for use with a vinylester matrix. Thus, it may be the fiber/matrix debonding controlled the toughness in the graphite reinforced specimen, and use of a better fiber sizing would perhaps produce values of G_c similar to those obtained for the glass reinforced specimen. This explanation is also consistent with the difference in G_c for the wet versus dry graphite specimens: the moisture reduces the residual thermal stresses at the fiber/matrix interface as well as provides some plasticization, and hence toughening of the matrix and fiber/matrix interface.

Tests of the glass reinforced laminates at the remaining environmental conditions produced relatively flat R curves, similar to those shown in Figure 11. Thus, for any condition, the mean toughness value was defined as the average from all specimens and all crack lengths at that condition. These results are presented in Figure 13. Here, the discrete symbols represent the mean of those specimens tested at each condition, and the error bars present ±1 standard deviation. Plotting the results in this manner, but separating out the data from specimens taken from panel 1 versus those from panel 4 evidenced no neither significant nor consistent panel-to-panel variation.

Figure 13 shows that the toughness of the glass reinforced sandwich laminates decreases with decreasing temperature. In view of the scatter, the sea water has no effect at -20C, 0C or 20C. Although it appears that there may be an effect of sea water saturation at -40C, recall that there were only three specimens tested at the -40C dry condition. This may be the reason that the standard deviation for the dry data is relatively small at this temperature. Thus, it is likely that there is no effect of moisture at any temperature in this material system.

<u>Conclusions</u>

The conclusions from this task are as follows:

- The improved MP test method works extremely well for assessing the effects of temperature and moisture on the deboning toughness of sandwich laminates.
- For the materials studied, glass reinforced sandwich laminates showed a higher debonding toughness than those with graphite reinforcement. However, it is quite likely that this was due to the fiber sizing that was used with the graphite fabric. One would expect that a better sizing would produce toughnesses similar to those obtained from the glass reinforced specimens.
- The toughness of the glass reinforced sandwich laminates studied steadily increases with increasing temperature over the range -40C to +20C. The toughness is insensitive to whether or not the specimen was sea water saturated over this temperature range.

Overall Conclusions

Significant research progress has been made during the past six months of research, and the overall research program is on track for completing all of its stated objectives during December 2008. This will complete the period of work of the overall study.

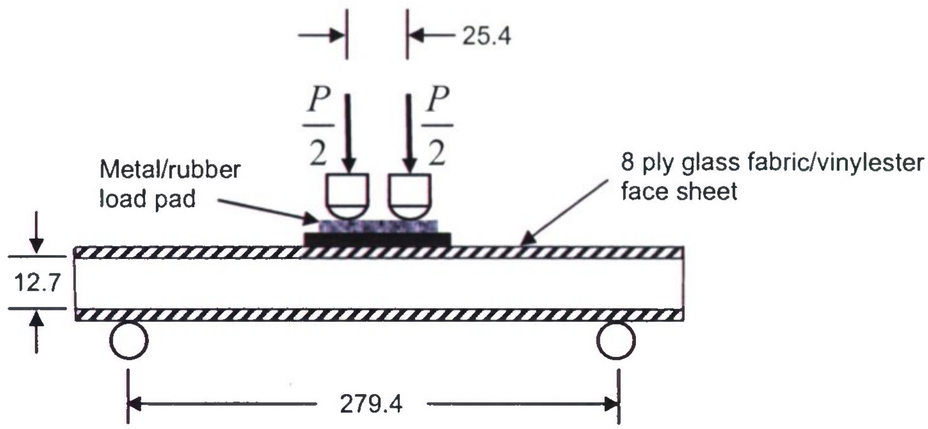

Figure 1. Schematic of bending test geometry (all dimensions are in mm).

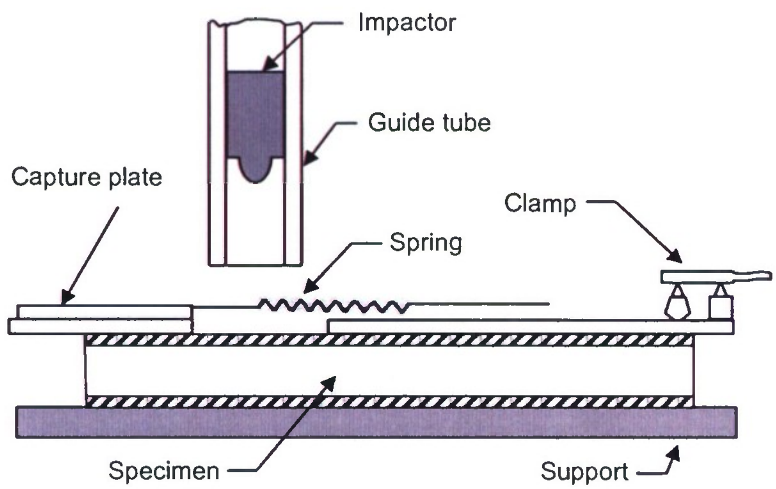

Figure 2. Schematic of impact fixture.

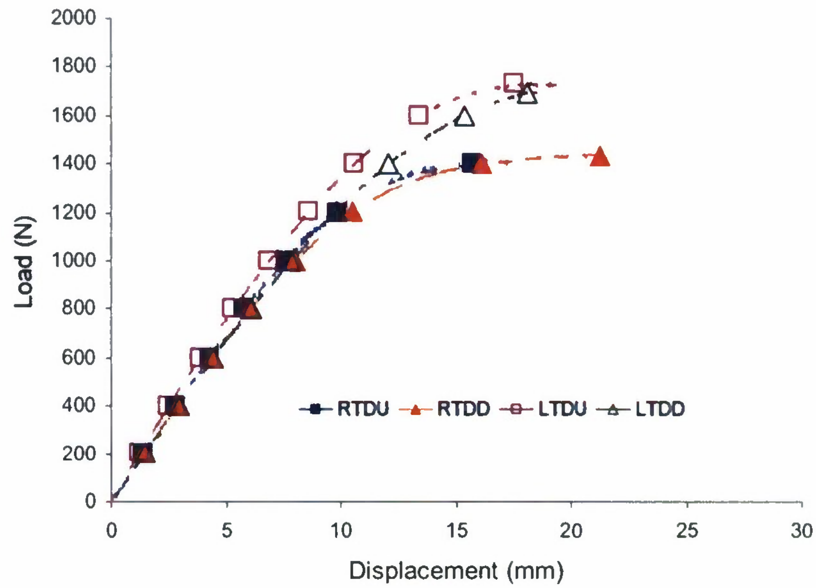

(a)

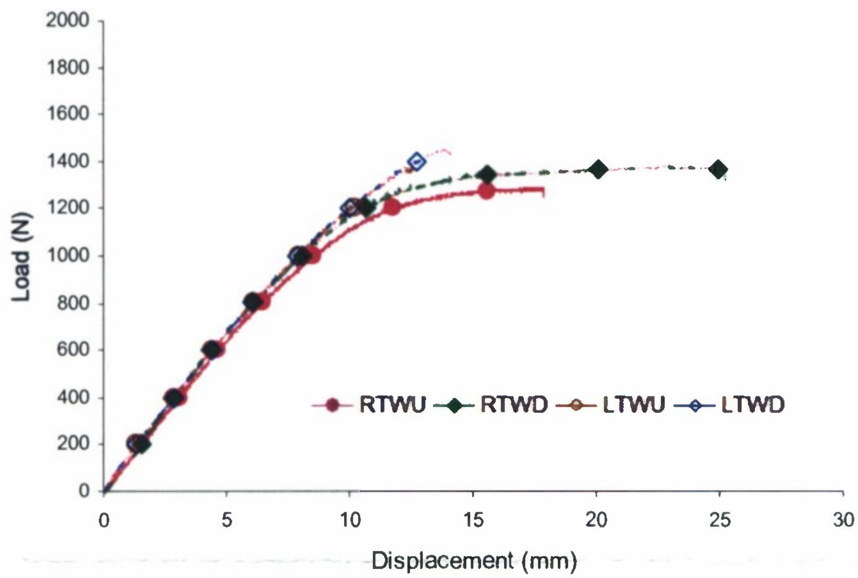

(b)

Figure 3. Typical load versus displacement plots.

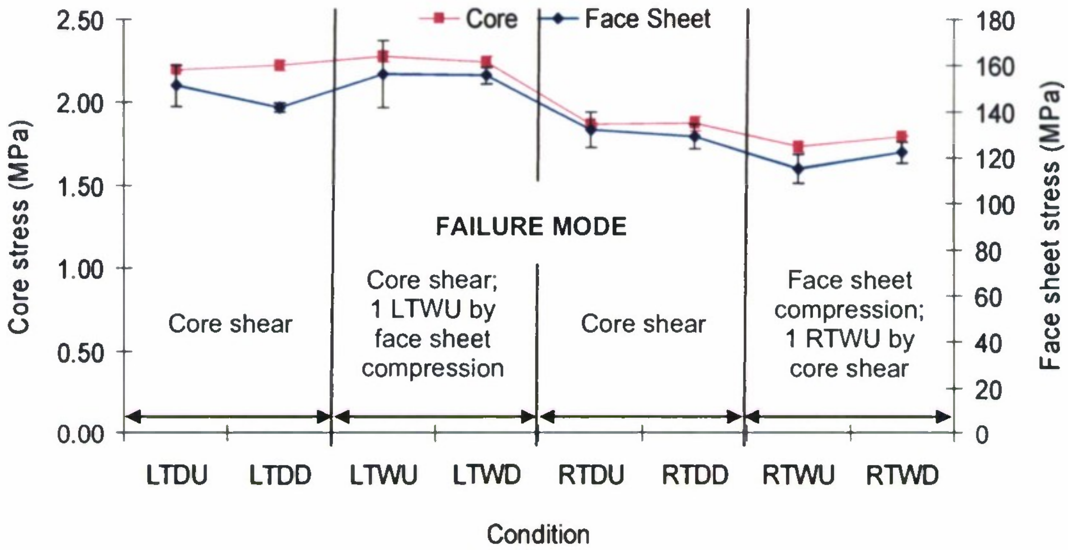

Figure 4. Static test results.

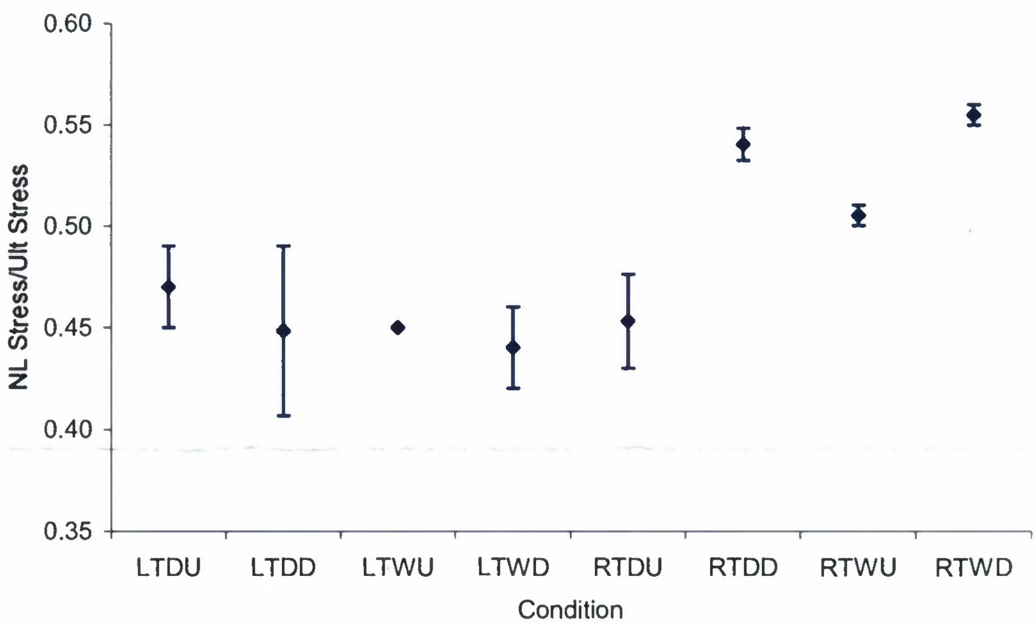

Figure 5. Ratio of nonlinear point stress to ultimate strength as a function of condition.

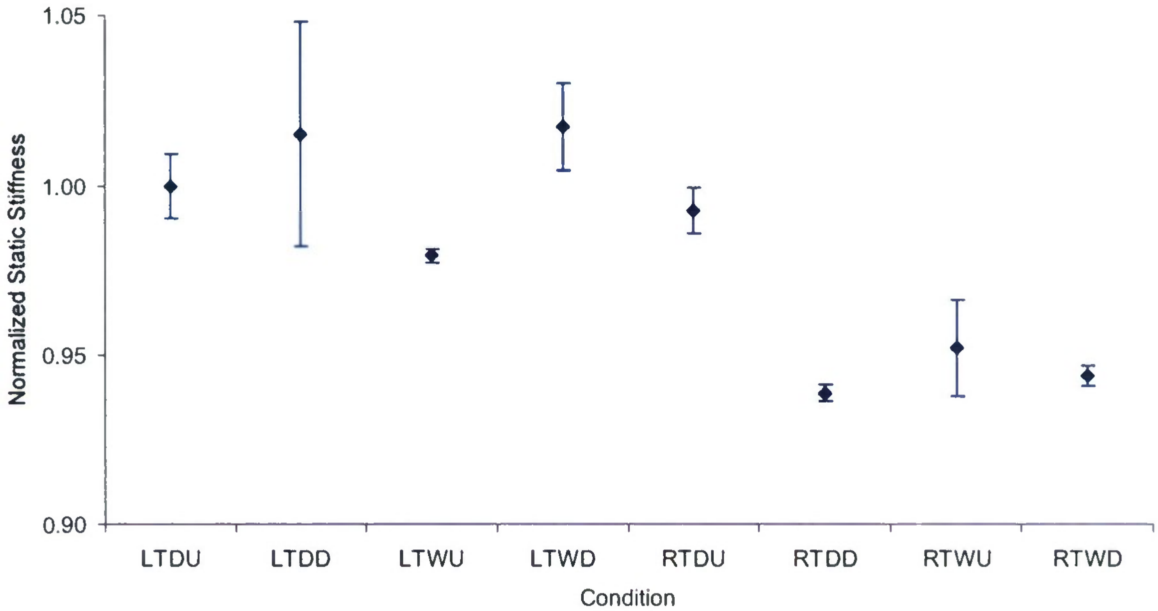

Figure 6. Normalized static stiffness versus condition.

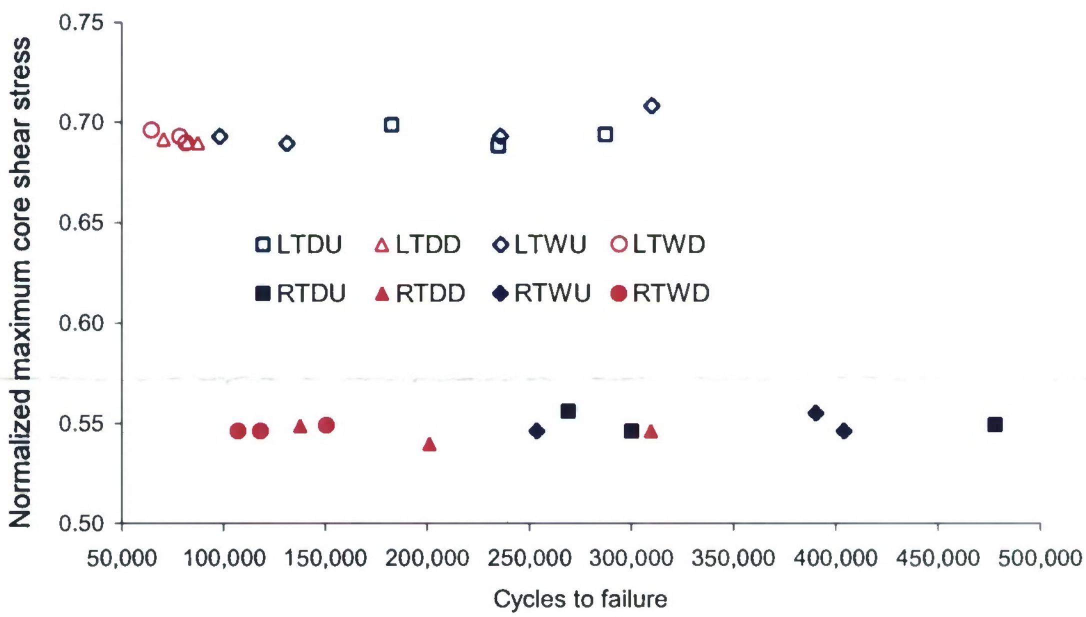

Figure 7. Normalized maximum core shear stress versus cycles to failure.

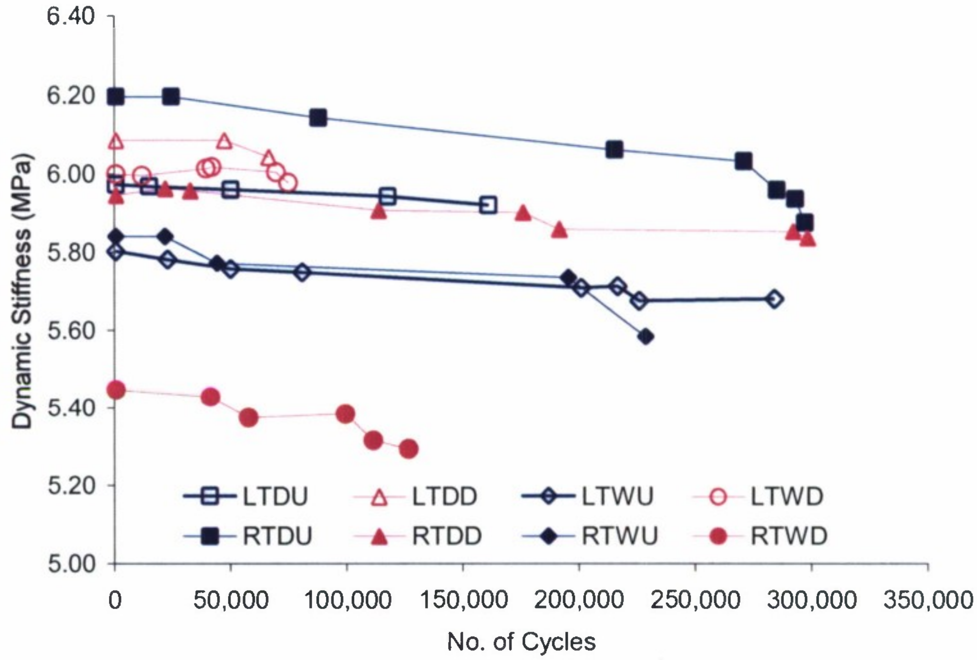

Figure 8. Typical plots of dynamic stiffness versus number of cycles.

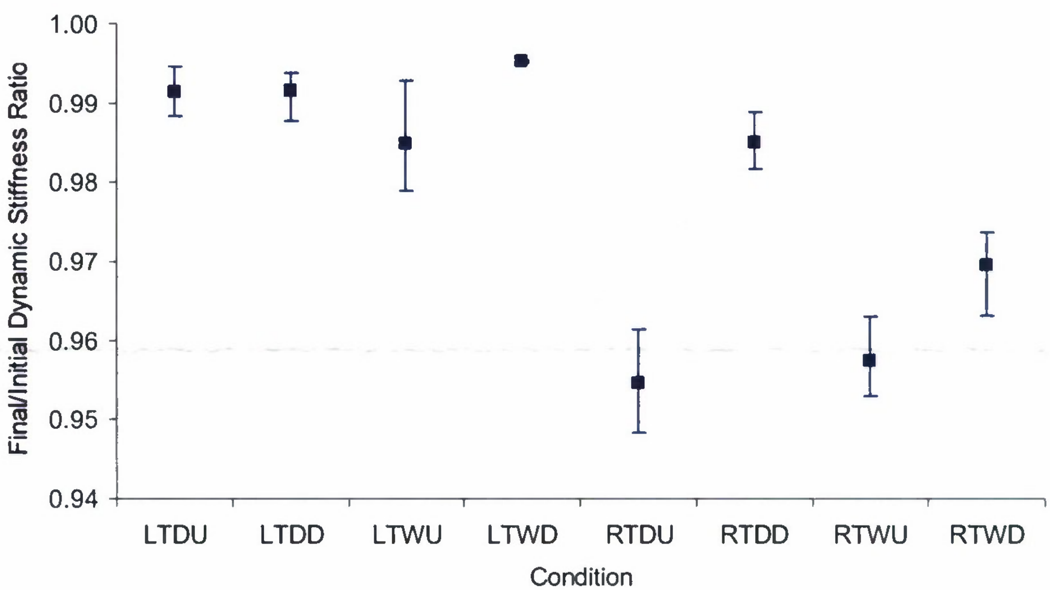

Figure 9. Ratio of final to initial dynamic stiffness as a function of test conditions.

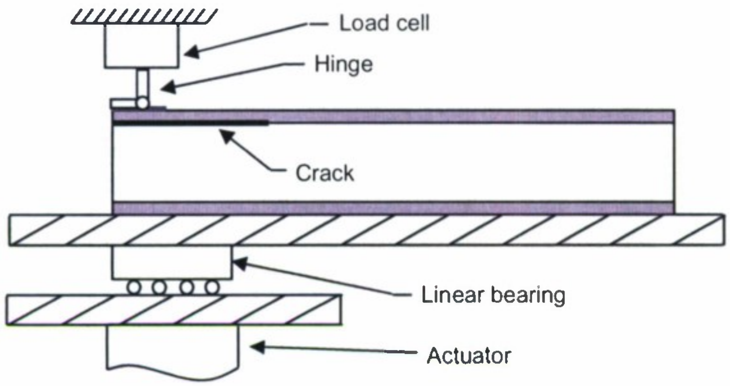

Figure 10. Schematic of the modified peel test.

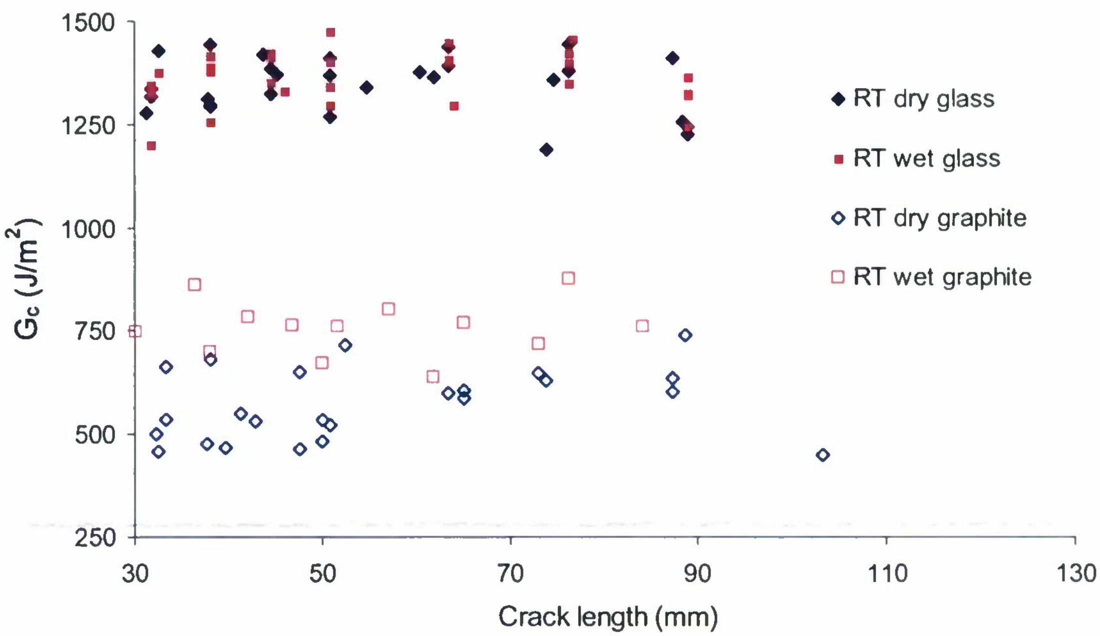

Figure 11. Resistance curves from room temperature tests.

(a)

(b)

Figure 12. Edge views of specimens during the test. (a) Glass reinforcement. (b) Carbon reinforcement.

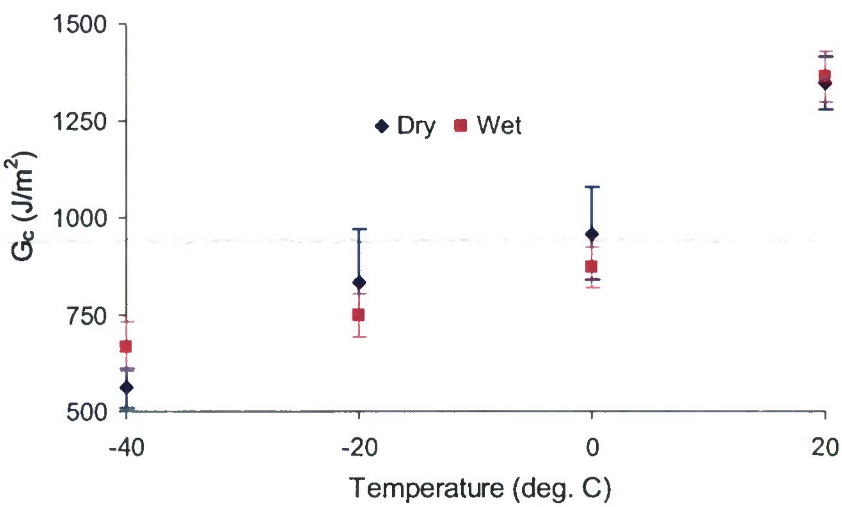

Figure 13. Mean toughness results from glass reinforced sandwich laminates.

APPENDIX

An Improved Methodology for Measuring the Interfacial Toughness of Sandwich Beams

Qida Bing and Barry D. Davidson

To Appear in

Major Accomplishments in Composite Materials and Sandwich Structures – An Anthology of ONR Sponsored Research

I.M. Daniel, E.E. Gdoutos, and Y.D.S. Rajapakse, Editors

An Improved Methodology for Measuring the Interfacial Toughness of Sandwich Beams

Qida Bing and Barry D. Davidson

Department of Mechanical and Aerospace Engineering

Syracuse University, Syracuse, NY 13244

Abstract Existing interfacial toughness tests are evaluated for their aeeuraey and suitability for application to a wide range of sandwieh struetures and environments. It is shown that geometric nonlinearities and/or axial load coupling can cause errors in the perceived toughness as obtained by many of these tests and their associated data reduction methods. A previously proposed modified peel test is selected to eliminate the effeet of axial load and a new, modified beam theory based method of data reduetion is developed. Experiments and nonlinear finite element analyses are used to show that this approach produces highly aeeurate values of toughness, even in the presence of geometrically nonlinear behaviors. Meehanieally attaehed loading tabs are deseribed, allowing the test to be used for a wide variety of structures under various simulated usage environments.

1 Introduction

Interfaeial eraek growth is a critieal mode of failure for foam core eomposite sandwich structures. Correspondingly, a large number of tests have been used to investigate interfacial growth behaviors and to determine the associated fracture toughness. Test methods that have been used or proposed include the cracked sandwich beam (also referred to as the asymmetrie double eantilever beam) [1-4], the modified cracked sandwich beam [5-10], thc tilted sandwieh debond [11-15], modified peel [16,17], eenter-notehed flexure [18-20], single eantilever three-point bend sandwieh [21], single cantilever beam sandwich [22] and the shear three-point bend sandwieh test [23,24]. The tilted sandwieh debond (TSD) test may be used at various tilt angles; it has the maximum amount of opening mode at a tilt angle of 0°, and the amount of shear increases as the tilt angle increases. The shear three-point bend sandwich tcst is a shear-dominated test. The remaining test methods, including the TSD at 0°, are aimed at obtaining toughness under primarily opening mode conditions. However, there currently is no consensus on preferred test methods, nor has there been a eomprehensive assessment of the accuracies of the various tests. This creates difficulties in choosing a method for material characterization. It also complicates the usage of material data that is presently available, as it is unclear whether results by the various test methods can be directly compared.

In view of the above, the goal of this study was to choose or develop an interfacial toughness test for sandwich structures, and an associated data reduction method, that could be used to obtain highly accurate toughness data under primarily opening mode conditions. Further, in support of on-going research, the method was to be applicable to a wide range of materials and environments, including both dry and seawater saturated laminates tested from +20 to -40°C. In addition to accuracy and environmental suitability, a secondary criterion related to required face sheet thickness, i.e., all other things being equal, the ability to test laminates with relatively thin face sheets reduces the overall manufacturing burden of a test program.

To address the above, a combined numerical and experimental approach is utilized, where finite element (FE) analyses are used to model a series of tests and perform virtual experiments. The trends and conclusions from this FE study are then validated through physical testing.

2 Test Methods Considered

An initial evaluation was first performed on those test methods described above that produce primarily opening mode fracture. The goal of this evaluation was to select a limited number of methods for more in-depth study. The cracked sandwich beam (CSB) test was first considered. Due to its asymmetric geometry, the CSB is an inherently nonlinear test [25]. The amount of nonlinearity depends on the bending stiffness mismatch between the two cracked regions and may lead to large rotations of the specimen. This significantly complicates data reduction, and makes it quite difficult to accurately extract the fracture toughness, G_c. It also often produces large face sheet deformations that result in compression failures. For these reasons, the CSB test was not chosen for consideration.

The modified cracked sandwich beam (MCSB) test, shown in Figure 2.1.a, was developed to overcome the difficulties associated with the CSB. As shown in the figure, in the MCSB the free end of the specimen is constrained from rotation. Although a small amount of nonlinearity was often observed in the load versus deflection data from the MSCB [6,7], a compliance calibration method of data reduction was judged to provide accurate toughness values [9]. Compliance calibration (CC) is an attractive method of data reduction, as it only assumes linear elastic behavior and self-similar crack advance. The former assumption can be verified through examination of the load-displacement data, and the latter can be validated through crack length measurements at both edges of the specimen. When these conditions apply, CC is generally considered to produce highly accurate values of G_c. The MSCB was therefore chosen for additional study.

The TSD (hereafter used to refer to the TSD at 0°), shown in Figure 2.1.b, is quite similar to the single cantilever beam sandwich test. The TSD is perhaps preferable, as it eliminates the flexural response of the uncracked region, the specimen is a bit shorter, and the bonded area of the specimen is larger than in the single cantilever beam sandwich test. It also appears that the TSD has been more widely used. For these reasons, the TSD was chosen for additional study. The modified peel (MP) test, shown in Figure 2.1.c, is similar to the TSD, but a linear bearing is used to prevent any axial force from being developed. As will be shown subsequently, evaluation of this test was necessary due to the problems that are created by the axial force in the MSCB and TSD tests.

The two remaining methods, the single cantilever three-point bend sandwich and the center-notched flexure test were not evaluated. The former test has not been used extensively, and the work performed on the tests above indicated that it likely would not produce any significant advantages. The latter test was not chosen for further study due to its complexity, issues associated with having two crack tips, and its relatively limited usage.

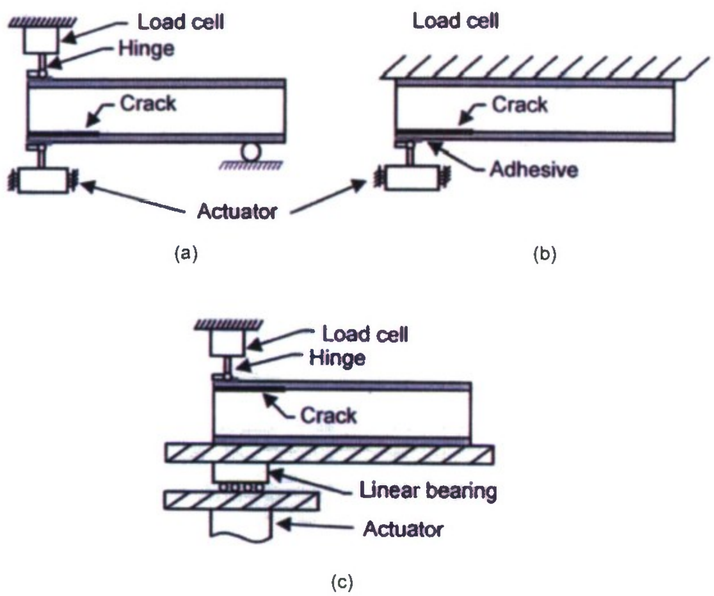

Fig. 2.1. (a) MSCB, (b) TSD at 0°, and (c) MP tests.

3 Geometries Considered

The three test methods chosen for in-depth evaluation are presented in Figure 2.1. All specimens considered in the finite element (FE) and experimental studies were 25.4mm wide with 25.4mm thick DIAB Divinylcell H100 PVC foam core. The experimental study considered 6, 12 and 18 ply thick face sheets comprised of BGF 7532 plain weave glass fabric with an areal weight of 241 g/m^2, whereas the FE study considered specimens with both woven glass and woven carbon face sheets that were 6 and 12 plies thick. All test specimens were manufactured by vacuum assisted resin transfer molding [5] using Derakane 411-350 vinylester resin. The 6 ply face sheets used a $[0/90/0]_s$ stacking sequence, the 12 ply sequence was $[0/90/0/0/90/0]_s$, and the 18 ply layup was $[0/90/0/90/0/90/0/90/0]_s$. Here, 0° is defined to be the warp direction and corresponds with the direction of crack advance. During manufacture, a 75mm long, 13μm thick teflon insert was placed at one end of the panel at the interface between the core and one of the face sheets to serve as a starter crack.

4 Finite Element Modeling

Linear and nonlinear (NL) FE analyses of the test geometries shown in Figure 2.1 were conducted. Although loading hinges are shown in this figure, loading blocks were also considered but were shown to considerably increase the nonlinearities that were observed. Thus, all results that are presented in this work are for loading hinges. The material properties used for the various constituents are presented in Table 4.1. As indicated, two types of glass face sheet and one type of carbon face sheet were considered, for which the planar modulus and Poisson's ratio are presented. Various choices of physically realistic through-thickness and shear modulus were evaluated for these materials and were found to have no influence on the conclusions that follow. The core, adhesive and loading hinge materials were all modeled as isotropic. The properties for glass face sheet (2) correspond to the specimens that were tested in this study, and the modulus that is presented corresponds to that obtained from flexural tests.

All FE models were constructed and analyzed using Abaqus™ V6.7. The core, face sheets, adhesive layer, and loading hinges were all discretely represented. The adhesive thickness was always modeled as 0.25mm thick. This was based on the experiments that were conducted, where glass beads of this diameter were mixed in with the adhesive when bonding. In accordance with the experimental set-up, the loading hinges were 12.7mm long and 1.52mm thick. The hinge pin was oriented on the side of the hinge closer to the crack tip and had a diameter of 3.18mm. Based on the test specimens that were manufactured, the 6 ply specimens were modeled as 1.45mm thick, and the thickness of the 12 ply specimens was taken as 2.51mm.

Table 4.1. Material properties.

	Glass face sheet (1)	Glass face sheet (2)	Carbon face sheet	Core	Adhesive	Loading Hinges
Modulus (GPa)	10.8	25.4	47.5	0.065	2.6	200.0
Poisson's ratio	0.11	0.11	0.04	0.337	0.30	0.29

Finite element meshing was performed primarily using two-dimensional, four-noded, plane stress elements, with a few triangular elements in the region where the hinge flange connected to the pin and in other transitional locations. An extensive mesh convergence study resulted in a mesh with square elements at the crack tip with edge lengths of approximately 0.081mm. Ten rows of these elements were placed on either side of the crack, i.e., within the face sheet and core. This refined region extended 3mm in either direction from the crack tip. Away from the crack tip, 6 elements were used through the thickness of the 6 ply face sheets, 12 were used through the thickness of the 12 ply face sheets, and 2 elements were used through the thickness of the adhesive. The loading hinges used 3 elements through their thickness with a length-to-height ratio of approximately 1.0. Boundary conditions were imposed in accordance with the physical tests of Figure 2.1. For the MSCB, the support roller at the uncracked end of the specimen was modeled as a rigid body. The contact between the roller and the specimen was frictionless with contact elements that were 1 ply thickness in height and just less than 1mm long.

Because crack advance occurred at a bimaterial interface, only total energy release rate (ERR) was evaluated. Linear mesh refinement studies showed that the mesh described above was sufficient to guarantee convergence in the ERR as determined by the virtual crack closure technique (VCCT) [26]. However, convergence studies with the NL models showed that the 4-noded elements evidenced extensive drawing and distortion at the crack tip, and the VCCT did not produce converged results. For this reason, the J-integral approach was used to extract G. Comparisons of J with G as determined from a global energy balance approach indicated that this method gave highly accurate results and remained converged with increasing mesh density. Thus, all results for ERR were determined via J, which was considered the "true ERR." Similar to the study of Ref. [27], these results were then compared to those from various simulated data reduction techniques for the materials in Table 4.1. Crack lengths from approximately 15 to 86mm were considered, with focus on specific crack lengths, a_o, of 25.4mm, 50.8mm and 76.2mm. Simulated CC was always performed by fitting compliance values from 5 different crack lengths. Specifically, the load versus deflection results were used from FE runs at a_o, $a_o \pm$ 5mm, and $a_o \pm$ 10mm to obtain compliance, and then the ERR, G, was obtained using the relation [28]

$$G = \frac{P^2}{2B}\frac{\partial C}{\partial a} \tag{4.1}$$

where P is the load, C is the compliance, B is specimen width and a is crack length. For these comparisons, various toughness values between 350 and 1400 J/m^2 were assumed. For example, if G_c=350 J/m^2, then the load versus deflection results at the 5 crack lengths considered for CC would be examined up to this ERR. For the specimens with 12 ply face sheets, the load versus deflection results were quite linear over this range at all crack lengths. In these cases, there was no problem defining compliance, C(a) would be curve-fit with an appropriate expression, and the value of load that corresponded to J=350 J/m^2 would be used to evaluate the CC method of data reduction using Eq. (4.1). In these situations, G by CC and J were found to be quite close. A similar approach would be used at higher values of assumed toughness. However, as the assumed value of G_c increased, nonlinearities began to become evident in the load versus deflection results. Unless otherwise stated, in these cases the compliance was obtained from the initial, linear portion of the curve. Here, the correspondence between G by CC and J was often poor. The associated physical problem is that, in practice, when geometric nonlinearities can occur and cause errors in the perceived toughness, then a simple criterion should be available for use in the interpretation of experimental results. This led to another measure by which the various tests and associated data reduction methods were evaluated: whether such a criterion could easily be found. Otherwise, it will be difficult to use the chosen approach with high confidence for a wide variety of geometries and environments.

5 MSCB Evaluation

Initially, the MSCB test appeared the most promising. It is a simple test to run and various data reduction methods have been evaluated [9]. However, exploratory experiments on MSCB specimens evidenced a host of problems, including perceived toughnesses that depended strongly on face sheet thickness and crack length, bond line failures for many of the load tabs, and compression readings from the load cell at long crack lengths in the 6 ply specimens. It was hypothesized that these behaviors were due to a combination of the axial constraint and NL effects induced by large deformations. That is, the schematic representation of the MSCB test shown in Figure 2.1.a represents the typical situation in a standard load frame. Figure 5.1 shows the forces on the specimen, where the subscript "v" is used for "vertical." The axial force arises because the lower loading pin wants to move to the right as a result of the horizontal shortening of the compliant (lower) leg as it deflects. However, the stiff upper leg does not deflect appreciably, and rotation of the specimen is constrained. Therefore, a tensile force is created in the more compliant leg. By equilibrium, this gives rise to an equal magnitude compression force in the stiff leg. The vertical force in the uncracked region arises to counteract the moment created by the axial loads. For small deformations, linear FE analyses predict these forces reasonably well, but NL effects become significant as the opening displacement reaches only a small percentage of the vertical distance between pins in the undeformed condition. Note also that large values of the axial force are consistent with the observations of load tab debonding. Further, a large axial force will cause a large value of $P_{uncracked}$. If $P_{uncracked}$ becomes sufficiently large, the direction of the vertical force at the load cell will change, i.e., a compressive load cell reading will be obtained, despite the fact that an opening load is applied at the actuator. This corresponds with the observed behaviors and was confirmed by NL FE analysis. Typical results are presented in Figure 5.2, which shows the relationship between reaction forces for an MSCB specimen with 12 ply glass face sheets at different crack lengths. It is observed that the reaction force that will be measured is dramatically different than that applied at the actuator. This can cause the perceived value of toughness to differ appreciably from the true value, and the difference will be a function of specimen thickness, material properties, and crack length. Although this problem could be addressed by mounting a load cell on the actuator, we considered common data reduction techniques [9] applied to the NL FE results and generally found poor agreement with G as determined from J. These difficulties caused us to shift focus to the TSD and MP tests.

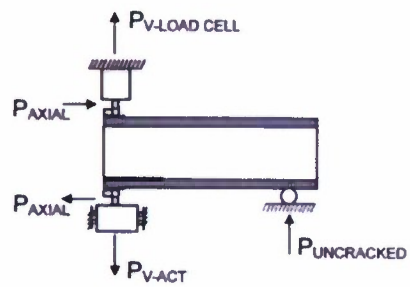

Fig. 5.1. Forces on the MSCB specimen

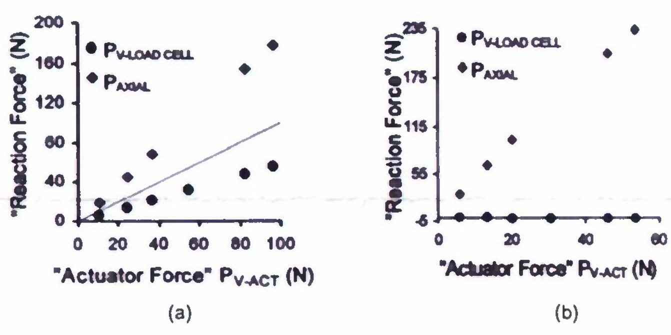

Fig. 5.2. Reaction forces for 12 ply MSCB. (a) 25.4mm, (b) 76.2mm crack length.

6 Preliminary Evaluation of the TSD Test

A preliminary evaluation of the TSD test indicated a number of potential problems. First, FE analyses indicated that the magnitude of the axial force developed in the TSD is similar to that which occurs in the MSCB for the same specimen geometry and applied load. Despite this, for certain test geometries, such as a relatively stiff cracked leg, a short crack length and a moderate toughness, it was found that the load-deflection response will remain reasonably linear and CC will produce accurate values of G_c. The problem here is that the mode mixity is changing with increasing load. For interfaces that have a higher toughness under shear-dominated loading, this will affect G_c, and the interpretation of this effect will be quite difficult. For test specimens with more compliant cracked regions and/or a high interfacial toughness, nonlinearities were observed in the NL FE load versus deflection results. In these cases, the accuracy of G_c as determined by the CC method could be quite poor. Further, both of the above scenarios are influenced by the introduction of extension rods, which are needed to perform tests within an environmental chamber, and which make the effect of the axial force very difficult to quantify in any meaningful way. Finally, there is the required bonding of the lower portion of specimen to a rigid surface, which may be problematic under certain environmental conditions. That is, as will be described subsequently, methods of mechanically attaching both the hinge and base that are relatively insensitive to environment were developed for the MP test, but the axial force in the TSD may cause the solution for the base region to be inappropriate for this test. Nevertheless, to better understand these issues, a decision was made to move forward with experimental evaluations of the TSD using the recommended method [11] of data reduction as well as a few variations. A modified beam theory based method of data reduction, similar to that described below for the MP test, was also considered for the TSD. However, due to the issues described above, this only met with limited success and is not described.

7 Data Reduction in the MP Test

A CC method of data reduction method was originally introduced for the MP that is identical to that used for composite double cantilever beam specimens [16]. Here, it is assumed that $C=Ra^n$, where R and n are obtained from a least-squares curve fit of the C(a) data. This expression for C is substituted into Eq. (4.1) to obtain a "load only" (LO) method of data reduction. A "load-deflection" (LD) method may be obtained by assuming that $\delta_c(a)=C(a)P_c(a)$, where δ_c is the critical deflection and P_c is the critical load. The resulting expressions are given by

$$G_{LO}^{DCB-CC} = \frac{P_c^2 Rna^{n-1}}{2B} \quad ; \qquad G_{LD}^{DCB-CC} = \frac{nP_c\delta_c}{2Ba} \tag{7.1}$$

These methods were evaluated using the NL FE results. Even for geometries where the load-deflection plots were essentially linear, it was found that both expressions gave relatively poor correlation with G from J. This was particularly true at the two shortest and two longest crack lengths used for CC, where the shape of the curve fit has the largest influence on slope. Thus, other curve-fits were considered. These consisted of 2nd, 3rd and 4th order polynomials in crack length and the "CC1" and "CC2" expressions typically used for the end-notched flexure test [27]. Here, for CC1 it is assumed that $C = A + ma^3$, and for CC2, $C = C_o + C_1a + C_2a^3$. Overall, the 3rd order polynomial and CC2 gave the best results, but G_c as determined by these methods exhibited errors on the order of 10% at the few shortest and longest crack lengths. When considering specimens where geometric nonlinearities occurred, for example for G_c = 1100 J/m^2 for any of the 6 ply face sheet specimens or for the 12 ply face sheet specimen constructed from glass fabric (1), all of the CC methods were very poor.

In view of the above, it was determined that a more robust method of data reduction was required. To this end, the modified beam theory (MBT) based LO and LD methods of data reduction developed for composite double cantilevered beam specimens [29] were modified for use with the MP test. Considering that only one cracked leg of the cracked sandwich beam is displacing in the MP test, the expression for ERR by the two methods are given by

$$G_{LO}^{MBT} = \frac{6P_c^2(a+\chi h)^2 F}{B^2h^3E_{1f}}; \quad G_{LD}^{MBT} = \frac{3P_c\delta_c}{2B(a+\chi h)}\frac{F}{N} \tag{7.2}$$

where h is the face sheet thickness and E_{1f} is the flexural modulus. The expression for G by the LO method for the MP test differs by a factor of 2 from the expression in [29] due to the fact that only one cracked leg of the cracked sandwich beam is displacing. However, the displacement of only a single leg enters into the LD expression and this expression is therefore unchanged from that in [29]. The parameters F and N correct for the reduction in moment at the crack tip due to face sheet shortening and the presence of a load tab, and are given by

$$F = 1-\frac{6}{5}\left(\frac{\delta}{a}\right)^2 - \frac{3l_1\delta}{a^2};$$
$$N = 1-\left(\frac{l_2}{a}\right)^3 - \frac{9}{4}\frac{\delta l_1}{a^2}\left[1-\left(\frac{l_2}{a}\right)^2\right] - \frac{36}{35}\left(\frac{\delta}{a}\right)^2 \tag{7.3}$$

Here, δ is the deflection, l_1 is the distance from the center of the loading pin to the mid-plane of the delaminated face sheet, and l_2 is half of the height of the end tab. If a hinge is used to introduce the load, then $l_2 = 0$. These expressions are also modified from those presented in [29] to account for the fact that only a single leg is displacing. The crack length correction factor, χ in Eq. (7.2), accounts for crack tip rotations, shear deformations and the beam on an elastic foundation effect. Both E_{1f} and χ are obtained from the slope and interception of the experimentally determined $(C/N)^{1/3}$ vs a curve following an approach similar to that described in [29], but the following expression is used

$$\left(\frac{C}{N}\right)^{1/3} = \left(\frac{4}{Bh^3 E_{1f}}\right)^{1/3} (a + \chi h) \tag{7.4}$$

In the above, C is defined as the slope of the deflection versus load plot from the test at any given crack length.

The key practical issue that arises when implementing the above approach lies in the determination of E_{1f} and χ. As described above, to obtain these values, one first determines the compliance of the MP specimen at each crack length, a. However, since there will be some nonlinearity in the load versus deflection plots, one will obtain different values of compliance, C, depending on the load and displacement level used for the linear regression analysis used to obtain C. In theory, the parameter N is intended to account for this, but in practice, different values of E_{1f} and χ are obtained over different ranges of curve-fit. This effect is much more pronounced in the MP than in typical DCB testing because of the relatively larger deflections that occur, particularly with glass-reinforced face sheets at large crack lengths.

In order to address the above, of all the geometries that were considered, those that showed nonlinearity in the NL FE prediction for load versus deflection (P-δ) response were isolated. Various criteria for determining compliance were considered. Each was used to determine E_{1f} and χ by Eq. (7.4). The ERR was then determined by the MBT-LO and MBT-LD methods and compared to J. Methods considered for fitting the compliance included constant load, constant displacement, constant ERR, and various compliance offsets. Of the methods evaluated, the most accurate approach, as well as the one that would be most easily implemented in actual testing, was a "95% compliance offset" method. Here, the compliance from the initial portion of the δ versus P curve is computed and used to find the intersection of the loading line with the zero load point; in practice, this accounts for any initial nonlinear portion of the curve that is possibly associated with take-up of free play in the system. Next, a line of slope 0.95C (corresponding to a 5.2% stiffness increase) is projected from this intersection point until it intersects with the δ versus P curve. That is, the NL FE analysis predicts that the slope of the loading line will increase due to the stiffening effect associated with moment arm shortening. The portion of the δ versus P curve above any initial nonlinearities and up to this intersection point is used to compute C/N for use in Eq. (7.4). If there is insufficient stiffening for the 0.95C and the loading lines to intersect, then the entire loading line (excluding any initial NL region) is used for the determination of C/N.

To illustrate, Table 7.1 presents the error in the LO and LD methods of data reduction (i.e., in comparison to the results by J-integral) for glass (1) fabric and carbon fabric face sheets of 6 and 12 ply thicknesses with assumed values of G_c of

350 J/m^2 and 1100 J/m^2. The mean and minimum errors refer to the average and minimum values, respectively, from all crack lengths studied. The average and minimum values of F, Eq. (7.3), are also presented and are discussed subsequently. This table shows that ERRs obtained by LD method are slightly more accurate than by the LO method. Since the carbon face sheets are significantly stiffer, little nonlinearity was displayed in the P-δ plots, and ERRs obtained by both methods are fairly accurate for all thicknesses and values of G_c. However, for glass face sheets in a material with G_c = 1100 J/m^2, neither method is capable of extracting G_c with extremely high accuracy. Thus, in this type of a situation, testing specimens with 12-ply thick face sheets would be recommended.

Table 7.1. Errors from LO and LD data reduction methods.

			Glass face sheet				Carbon face sheet			
Method	Face sheet thickness	G_c (J/m^2)	Mean error (%)	Max error (%)	F Avg	F Min	Mean error (%)	Max error (%)	F Avg	F Min
LO	6-ply	350	-2.84	-3.40	0.812	0.756	-0.21	-0.97	0.912	0.885
LO	6-ply	1100	-9.81	-11.47	0.581	0.432	-3.94	-5.70	0.800	0.703
LO	12-ply	350	-1.50	-2.12	0.934	0.914	-1.09	-1.82	0.969	0.962
LO	12-ply	1100	-5.83	-6.57	0.809	0.772	-2.89	-3.90	0.916	0.899
LD	6-ply	350	-2.56	-2.95	0.812	0.756	-0.73	-1.47	0.912	0.885
LD	6-ply	1100	-8.00	-10.69	0.581	0.432	-2.62	-3.97	0.800	0.703
LD	12-ply	350	-1.79	-2.15	0.934	0.914	-1.21	-1.78	0.969	0.962
LD	12-ply	1100	-5.20	-5.38	0.809	0.772	-2.72	-3.45	0.916	0.899

The above discussion brings up the interesting problem that, in practical situations one must know – without the benefit of NL FE analyses – what the accuracy of the method is. This information would be critical to deciding whether or not G_c could be extracted accurately from tests of sandwich structure of a given material and face sheet thickness. Alternatively, one could think of this type of information as being used to design appropriate tests. To address this, various "cut-off" criteria were evaluated. Methods considered included expressions based on F, N, and various nondimensionalized displacements. Once a candidate approach was found, additional geometries were then analyzed to make sure that the chosen method would be widely applicable. The most promising method, and one that could also be easily implemented in practice, was based on the parameter F. This is illustrated in Figure 7.1. Figure 7.1.a presents the error in the ERR as predicted by the LD method for all cases considered, and similar results for the LO method are presented in Figure 7.1.b.

In practical applications, if one excludes results from tests where $F<0.73$ due to potential data reduction errors, then the worst-case error based on all of our simulations would be -5.4% if the LD method is used and -6.8% if the LO method is used. Referring once again to Table 7.1, it was found that F is less than 0.73 by both methods for all crack lengths for the specimens with 6 ply glass (1) fabric face sheets and a toughness of 1100 J/m^2. Thus, if one were to perform an experiment on specimens of this type, the first test (assuming growth over a range of crack lengths from ~25 to 75mm) would yield a mean value of F of around 0.58. Based on the cut-off criterion, this would provide the feedback that this test geometry is unacceptable. One would also expect to see reasonably large nonlinearities in the load versus deflection plots. For sandwich structure with 6 ply carbon fabric face sheets and a toughness of 1100 J/m^2, the NL FE results indicate that F will be greater than 0.73 for crack lengths less than approximately 74mm. Thus, if one was performing tests of this geometry, the cut-off criterion provides a means to know up to what crack length the values of G_c are expected to be reliable.

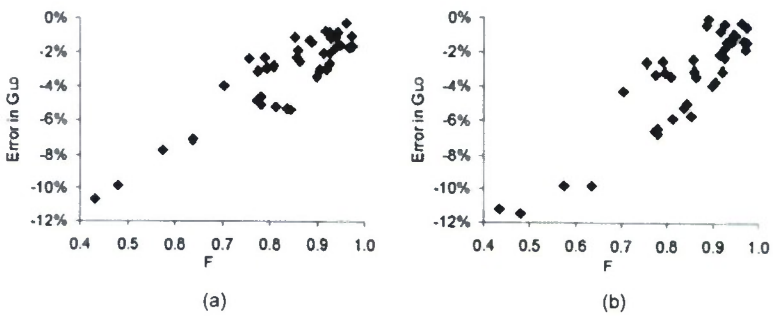

Fig. 7.1. Errors in ERR by (a) LD and (b) LO method for MP test.

8 TSD and MP Experiments

Prior to testing, marks were place on the edges of all TSD and MP specimens at specific distances ahead of the crack tip. During testing, the specimen was rapidly unloaded when the crack reached one of these marks. The crack length was then measured accurately at each edge, and the average of these measurements, along with the load at the instant that the test was stopped, were used in data reduction. In virtually all cases, the exact point of onset of advance from the teflon insert could not be identified, so this value was not used for the determination of toughness. Rather, when presenting resistance (R) curves, the first crack length corresponds to the first time the test was stopped. To eliminate any effects of panel-to-panel manufacturing variations, all specimens tested at a given thickness were cut from the same panel.

Figure 8.1 presents load versus deflection plots from MP and TSD tests of specimens with 12 and 18 ply thick face sheets. It can be observed that the MP tests (Figures 8.1.a and 8.1.d) are quite linear. The 12 ply TSD tests with an extension rod, Figure 8.1.b, were reasonably linear at short crack lengths, but became increasingly nonlinear as the crack extended. Increasing to an 18 ply thick specimen with an extension rod, Figure 8.1.e, improved the results considerably. As shown in Figures 8.1.c and 8.1.f, significant amounts of NL were observed in both the 12 and 18 ply TSD tests without extension rods, and it is likely that the CC method of data reduction is not applicable. In fact, when the CC method was applied, these tests gave a very different toughness and R curve than that obtained from the tests where the extension rods were used. As such, toughness data from the TSD tests without extension rods are not presented. It is pointed out that when testing the TSD specimens with extension rods, an in-plane deflection of the rod tips was quite visible due to the shortening effect and associated axial load.

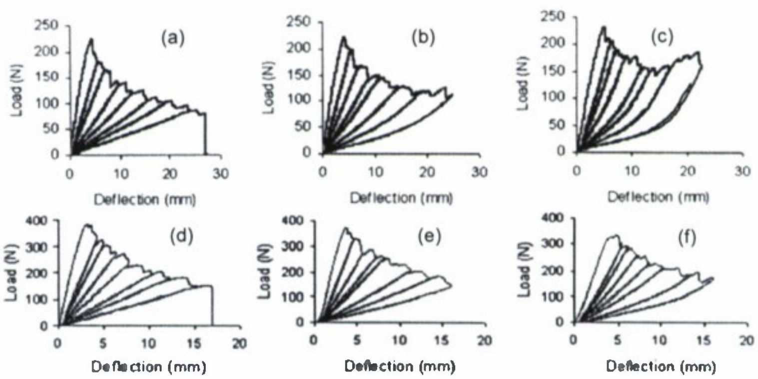

Fig. 8.1. Load versus defection plots. (a) 12 ply MP, (b) 12 ply TSD with extension rods, (c) 12 ply TSD, (d) 18 ply MP, (e) 18 ply TSD with extension rods, (f) 18 ply TSD.

The recommended data reduction method for the TSD test is a 2nd order polynomial [11]. This was based on a goodness of fit assessment, rather than through a supporting analysis that indicated the functional relationship of ERR on crack length. Thus, we considered 2nd, 3rd and 4th order polynomials. The corresponding goodness of fit (R^2) values were generally 0.998, 0.999 and 1.000, respectively. However, the resulting toughness values from the first 1-2 and last several crack lengths varied dramatically based on the curve fit that was chosen. Any significant NL in the load-deflection plot (e.g., at large a) accentuated these differences. Restricting consideration to only those crack lengths where the P-δ plots were essentially linear resulted in different toughness predictions by the various curve fits for only the first 1-2 and last 1-2 crack lengths considered. This is where the different curve fits have the most effect on the slope of the C versus a curve [cf. Eq. (4.1)]. Since it is unclear which curve fit predicts toughness accurately, in what follows

TSD toughness data are only presented from those crack lengths where good agreement in G_c was obtained from the various compliance fits.

Based on the NL FE evaluation, for the MP test, G_c was determined by the MBT-LD method. These agreed well with the MBT-LO results and, except for the first 1-2 crack lengths, with those from CC using a 3rd order polynomial or the CC2 curve fit.

Toughness results are presented in Figure 8.2.a for specimens with 12 ply thick face sheets and in Figure 8.2.b for specimens with the 18 ply face sheets. For both geometries, the range of "good data" is much larger from the MP than the TSD test. As is evident from a comparison of Figures 8.1.b and 8.1.e, more nonlinearity occurs in the P-δ data from the 12 than from the 18 ply TSD. Correspondingly, the range of R curve data by the TSD is longer for the 18 ply specimens.

Providing that extension rods are used with the TSD test, Figure 8.2 shows good correspondence for G_c by the MP and TSD tests of 18 ply specimens. Here, the TSD test produces essentially linear P-δ data. For the 12 ply specimens, the P-δ data from the TSD test evidence nonlinearities and, despite the measures employed to ensure accuracy, the TSD produces higher toughness values. In addition to the effects of the nonlinearity, it is possible that this is strongly influenced by the different mode mixity in the two tests. That is, the horizontal forces due to face sheet shortening that arise in the TSD causes it to have a greater shear component than the MP. This effect increases with decreasing face sheet thickness due to the associated increase in deflection at fracture.

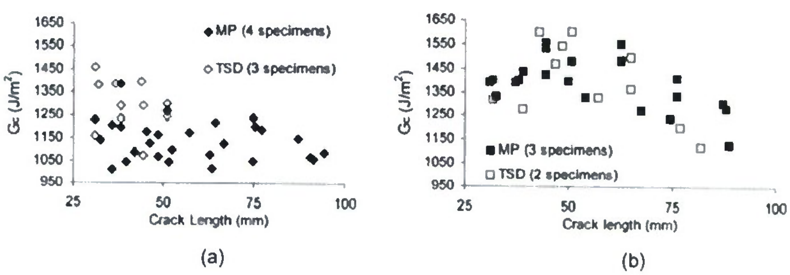

Fig. 8.2. Toughness results from MP and TSD tests with extension rods. (a) 12 ply. (b) 18 ply.

Considering the MP test results only, the mean toughness from all specimens at all crack lengths for the 12 ply specimens is 1138 J/m^2 with a standard deviation of 86.6 J/m^2. The mean from the 18 ply specimens is 21% greater, with mean and standard deviations equal to 1382 and 103.4 J/m^2, respectively. However, the difference between the 12 ply and 18 ply results do not necessarily reflect a thickness effect, as they are also affected by panel-to-panel variation. For example, in our current testing, we have obtained a mean toughness and standard deviation from specimens of a different 12 ply panel equal to 1355 and 61.8 J/m^2, respectively. In view of this, it appears that the entire difference between the 12 and 18 ply results could be due to manufacturing variations between panels.

9 Mechanical Attachments

As shown in Figure 9.1, the MP test may readily be used with mechanical attachments. Figure 9.1.a shows the hinge attachment. Here, a region of the core remote from the crack tip is cut away, and three fasteners and a backing plate are used to attach the hinge to the face sheet. The base plate attachment is shown in Figure 9.1.b. Wedge grips were machined with a step height just less than the smallest face sheet thickness that was tested. Each wedge is pressed into the core to a depth of approximately 2.5mm. Plastic shim stock is placed beneath the wedge to account for variations in face sheet thickness among specimens. Tests of specimens with these attachments versus those that had bonded connections showed no difference in toughness.

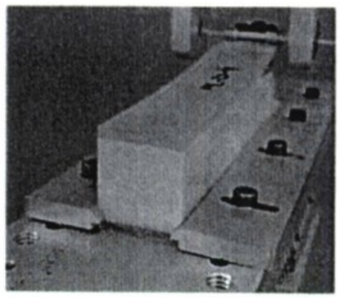

(a) (b)

Fig. 9.1. Mechanical attachments for the MP test. (a) Hinge. (b) Base.

10 Conclusions

The modified peel test with the newly developed modified beam theory based data reduction method has been shown to produce highly accurate values of interfacial toughness for sandwich structures with composite face sheets. The MP test provides a larger range of accurate crack growth data from debonding tests than that which can be obtained using existing methods. It also eliminates the need to interpret whether data from a given increment of crack advance are acceptable due to the possibility of errors in dC/da. These may arise due to the sensitivity of the derivative near the extreme values of crack length used for the C(a) fit and/or due to geometric nonlinearities that effect the load versus deflection data. Considering the associated cut-off criterion that was developed for tests that show nonlinear behavior, the MP eliminates the need for subjective interpretations on whether or not some or all of the data from any particular test is "acceptable." It also follows that the MP will allow the use of thinner face sheet specimens than existing test methods without a compromise in accuracy. Further, eliminating the axial load prevents toughness variations that may arise due to the associated change in mode mix with crack length. The MP is a predominantly opening mode test and should therefore provide a conservative measure of toughness for use in practical applications. Coupled with the method of mechanical attachment, the advantages of this test are quite significant, and serve to ensure that the MP test may be used for accurate determination of the interfacial toughness of all types of sandwich structures under a wide range of environmental conditions.

11 Acknowledgement

This work was supported by the Office of Naval Research under Contract N00014-07-1-0418, Dr. Yapa D. S. Rajapakse, Program Manager.

12 References

1. Prasad S, Carlsson LA (1994) Debonding and crack kinking in foam core sandwich beams-II Experimental investigations. Eng Fract Mech 47:6:825-841
2. Carlsson LA, Matteson RC, Aviles F, Loup DC (2005) Crack path in foam cored DCB sandwich fracture specimens. Compos Sci Technol 6:2612-2621
3. Grau DL, Qiu XS, Sankar BV (2006) Relation between interfacial fracture toughness and mode-mixity in honeycomb core sandwich composites. J Sandw Struct Mater 8:187-203
4. Matteson RC, Carlsson LA, Aviles F, Loup DC (2005) On crack extension in foam cored sandwich fracture specimens. In: Thomsen OT et al (eds.) Sandwich structures 7: Advancing with sandwich structures and materials, 7th edn. Springer, Netherlands
5. Smith SA, Emmanwori LL, Sadler RL, Shivakumar KN (2000) Evaluation of composite sandwich panels fabricated using vacuum assisted resin transfer molding. In: Proceedings of the 43rd international society for the advancement of material and process engineering conference, Anaheim CA
6. Smith SA, Shivakumar KN (2001) Modified mode-I cracked sandwich beam (CSB) fracture test. In: Proceedings of the 42nd AIAA/ASME/ASCE/AHS/ASC Structures structural dynamics and materials conference
7. Shivakumar KN, Smith SA (2004) In situ fracture toughness testing of core materials in sandwich panels. J Compos Mater 38:8:655-668
8. Shivakumar KN, Smith SA (2002) Influence of core density and facesheet properties on debond fracture strength of foam core sandwich composites. In: Sun CT, Kim H (eds) Proceedings of the American society for composites 17th technical conference, West Lafayette, Indiana
9. Shivakumar KN, Chen H, Smith SA (2005) An evaluation of data reduction methods for opening mode fracture toughness of sandwich panels. J Sandw Struct Mater 7:1:77-90
10. Kolat K, Neser G, Ozes C (2007) The effect of sea water exposure on the interfacial fracture of some sandwich systems in marine use. Compos Struct 78:11-17
11. Li X, Carlsson LA (1999) The tilted sandwich debond (TSD) specimen for face/core interface fracture characterization. J Sandw Struct Mater 1:1:60-75

12. Viana GM, Carlsson LA (2003) Influences of foam density and core thickness on debond toughness of sandwich specimens with PVC foam core. J Sandw Struct Mater 5:103-118
13. Majumdar P, Srinivasagupta D, Mahfuz H et al (2003) Effect of processing conditions and material properties on the debond fracture toughness of foam-core sandwich composites. Compos Part A: Appl Sci Manuf 34:1097-1104
14. Li X, Weitsman YJ (2004) Sea-water effect on foam-cored composite sandwich lay-ups. Compos Part B: Eng 35:451-459
15. Truxel A, Aviles F, Carlsson LA et al (2006) Influence of face/core interface on debond toughness of foam and balsa cored sandwich. J Sandw Struct Mater 8:237-258
16. Cantwell WJ, Davies P (1994) A test technique for assessing core-skin adhesion in composite sandwich structures. J Mater Sci Letters 13:203-205
17. Cantwell WJ, Davies P (1996) A study of skin core adhesion in glass fiber reinforced sandwich materials. Appl Compos Mater 3:407-420
18. Ratcliffe J, Cantwell WJ, (2000) A new test geometry for characterizing skin-core adhesion in thin-skinned sandwich structures. J Mater Sci Letters 19:15:1365-1367
19. Ratcliffe J, Cantwell WJ (2001) Center notch flexure sandwich geometry for characterizing skin-core adhesion in thin-skinned sandwich structures. J Reinf Plast Compos 20:11:945-970
20. Gates TS, Su X, Abdi F et al (2006) Facesheet delamination of composite sandwich materials at cryogenic temperatures. Compos Sci Technol 66:2423-2435
21. Cantwell WJ, Scudamore R, Ratcliffe J, Davies P (1999) Interfacial fracture in sandwich laminates. Compos Sci Technol 59:2079-2085
22. Cantwell WJ, Broster G, Davies P (1996) The influence of water immersion on skin-core debonding in GFRP-balsa sandwich structures. J Reinf Plast Compos 15:11:1161-1172
23. Carlsson LA, Sendlein LS, Merry SL (1991) Characterization of face sheet/core shear fracture of composite sandwich beams. J Compos Mater 25:101-116
24. Shipsa A, Burman M, Zenkert D (1999) Interfacial fatigue crack growth in foam core sandwich structures. Fatigue Fract Eng Mater Struct 22:2:123-121
25. Sundararaman V, Davidson BD (1997) An unsymmetric double cantilever beam test for interfacial fracture toughness determination. Int J Solids Struct 34:7:799-817.
26. Rybicki EF, Kanninen MF (1977) A finite element calculation of stress intensity factors by a modified crack closure integral. Eng Fract Mech 9:931-938
27. Davidson BD, Sun X (2006) Geometry and data reduction recommendations for a standardized end notched flexure test for unidirectional composites. J ASTM Int 3:9:1-19
28. Broek D (1986) Elementary engineering fracture mechanics. 4th rev edn, Kluwer Academic Publishers Inc
29. Hashemi S, Kinloch AJ, Williams JG (1990) The analysis of interlaminar fracture in uniaxial fibre-polymer composites. Proc R Soc London 427:173-199